J. Eur. Opt. Soc.-Rapid 10, 15002 (2015) [www.jeos.org]

Fourier ellipsometry – an ellipsometric approach to Fourier scatterometry

Peter Petrik,[1,*] Nitish Kumar,[2] Miklos Fried,[1] Balint Fodor,[1] Gyorgy Juhasz,[1] Silvania F. Pereira,[2] Sven Burger[3] and H. Paul Urbach[2]

[1] *Institute for Technical Physics and Materials Science, Hungarian Academy of Sciences, H-1121 Budapest, Konkoly Thege u. 29-33*

[2] *Optics Research Group, Department of Imaging Physics, Faculty of Applied Sciences, Delft University of Technology, P. O. Box 5046, 2600GA Delft, The Netherlands*

[3] *Zuse Institute Berlin (ZIB), Takustrasse 7, D-14195 Berlin, Germany*

[*] *Corresponding author: petrik@mfa.kfki.hu*

An extension of Fourier scatterometry is presented, aiming at increasing the sensitivity by measuring the phase difference between the reflections polarized parallel and perpendicular to the plane of incidence. The ellipsometric approach requires no additional hardware elements compared with conventional Fourier scatterometry. Furthermore, incoherent illumination is also sufficient, which enables spectroscopy using standard low-cost light sources.

Keywords:

Optical Metrology, Ellipsometry, Scatterometry, RCWA, Fourier Scatterometry, Sensitivity

1 Introduction

Optical scatterometry is used in numerous configurations [1–4] from monochromatic to spectroscopic, from reflectometric to polarimetric, from specular to angle resolved, from coherent to incoherent. In Fourier scatterometry, a focused spot is created by a high numerical aperture (NA) microscope objective (MO), and the scattered illumination is collected by the same MO [5]. In this configuration, each point of the back focal plane of the MO is uniquely related to a given reflection and azimuth angle. Fourier scatterometry allows the measurement of small and weakly reflecting samples over a wide range of reflection angles. Using high-NA MOs, the angles of reflection cover the range from 0 to over 70° (72° for NA=0.95), and the distance of the objective is only several hundred wavelengths from the sample surface. The whole back focal plane image that includes the response of the sample at all conical angles, can be recorded within less than a second.

By using coherent illumination and a scanning focused spot, the phase can be modulated and the phase difference between the overlapping orders can be determined [4,6,7], resulting in an increase in the sensitivity as compared to phase-insensitive incoherent Fourier scatterometry. A further advantage of the coherent illumination is that the size of the focused spot is much smaller (below one micron in the visible wavelength range).

The performance of coherent Fourier scatterometry can further be increased by combining it with interferometry [8]. Using interferometry, the complete scattering matrix is evaluated. The absolute phase distribution of the diffracted orders are retrieved using a known reference beam.

The ellipsometric approach [9–11] can be considered as a variation of the interferometric method, in which the reference beam for one polarization is that of the orthogonal polarization with regard to the plane of incidence. The material and structure related parameters determined by standard rotating analyzer or rotating polarizer ellipsometry are the ratio of the absolute value (tan[Ψ]) and the phase difference (Δ) of the complex reflection coefficients (r) of light polarized parallel (p) and perpendicular (s) to the plane of incidence:

$$\rho = \frac{r_p}{r_s} = tan(\Psi)e^{i\Delta}, \tag{1}$$

where ρ denotes the complex reflectance ratio.

The ellipsometric parameters can be determined by rotating a polarizer either on the input or on the output side of the setup, and analyzing the line shape of intensities as a function of the polarizer angle for each pixel. Compared to a basic Fourier scatterometric configuration, no additional optical components are required, and there is no need to measure the input field intensity and phase.

2 Principle of detection

The general configuration is shown in Fig. 1a. It is the same as for coherent Fourier scatterometry experiments [4,6,12]. The light is focused by an MO to the sample. At the back focal plane of the MO each point uniquely corresponds to a certain reflected angle from the illuminated spot. When imaging the BFP to the CCD, the intensity can be measured for each reflected angle. This configuration has been investigated in scanning spot [4,6,7,12,13] and interferometric [8,14] setups, for which a sensitivity increase between 2 and 8 has been revealed, depending on the measurement parameters and the sample. In case of Fourier scatterometric ellipsometry the only difference with regard to the above arrangement is that either the polarizer for the input beam (P1) or the polarizer for the output beam (P2) is rotated, and the intensity at each pixel of the camera is recorded (Fig. 1b).

In case of scanning spot Fourier scatterometry [4, 6, 7, 12, 13] and interferometric Fourier

scatterometry [8,14] the phase is measured between the reflected orders and with regard to a reference beam, respectively, whereas ellipsometric Fourier scatterometry measures the phase between the reflections of perpendicular polarizations. Fig. 2 shows the absolute values (top graph) and phases (bottom graph) of the complex reflection coefficient ratios for TE and TM polarizations (equivalent with $tan(\Psi)$ and Δ in Eq. 1, respectively) over an $NA = 0.9$ pupil area calculated using the rigorous coupled wave analysis (RCWA, [15]). The typical repeatability of phase (shown in the bottom graph of Fig. 2) by an ellipsometric measurement is approximately 0.001, which is more than 3 orders of magnitude better than the range plotted for $arg(r_{TE}/r_{TM})$.

3 Sensitivity

The increase in sensitivity can be determined by calculating the derivative of the merit function

$$\chi^2 = \frac{1}{N} \sum_{N}^{i=1} \left[y_i^{(m)} - y_i^{(c)} \right], \tag{2}$$

(where N is the number of measured ($y^{(m)}$) or calculated ($y^{(c)}$) data points), and using standard procedures of calculating the curvature and covariance matrices [7, 16, 17] from which the 90% confidence limits can be calculated. Usually the $y^{(m)} - y^{(c)}$ differences in Eq. 2 are divided by the measurement error of each $y_i^{(m)}$ data point, but in our case $y^{(m)}$ is replaced by simulation and this normalization is neglected. Consequently, the $y^{(m)} - y^{(c)}$ differences are calculated using $y^{(c)}$ values for small parameter changes around the nominal values of $y^{(m)}$.

The increase in sensitivity is defined as the ratio of the confidence limits with (σ_{ellip}) and without ($\sigma_{noellip}$) using the ellipsometric approach. Fig. 3 shows the RCWA calculations for a resist grating on a silicon substrate measured using a numerical aperture of 0.9. The top graph shows the sensitivity gain for the height and critical dimension parameters as a funcion of the height of the grating, whereas the sensitivity gain of the critical dimension parameter is plotted for a range of overlap parameters in the bottom graph. Generally, the uncertainty of the parameter fit is better (smaller) by a factor of 3-8 when using the ellipsometric approach, depending on the measurement and sample parameters. The same sensitivity calculations have also been performed for a 3D structure, as shown in Fig. 4. In this case we used finite element method (FEM) calculations by the JCMsuite software [18], which provides advantages compared to RCWA for 3D structures [19]. We investigated a hexagonal lattice of holes in Si with varied height and parameters described in the caption of Fig. 4. The increase in sensitivity is typically between 5 and 10, close to the values for the regular grating shown in Fig. 3.

4 Comparison

It has been shown in previous studies that involving the phase information in the measurement increases the sensitivity significantly [4, 6–8, 12–14]. The main methods investigated so far are summarized in Table 1. In case of the scanning spot method a coherent light source is applied, and the coherent superposition of overlapping orders is measured and calculated. The phase modulation is achieved by scanning the focused spot [6, 7, 12–14]. Since the interference pattern measured in the far field depends on the spot position very sensitively, this method can also be used for nanopositioning, i.e. for setting the spot position with nanometer accuracy.

In case of interferometric Fourier scatterometry (which can be combined with the scanning spot method) a coherent reference beam with phase modulation is used. [8]. Using this method, a sensitivity increase can be achieved also for gratings the illumination of which does not result in overlapping order. This is typically the case for gratings of which no overlapping order is present in the far field. For both of the scanning spot and the interferometric methods, the intensity and phase distribution of the incident beam over the pupil has to be measured and taken into account in the fitting procedure. Furthermore, the interferometric setup requires additional hardware elements compared to the scanning spot methods (providing the modulated reference beam).

In case of ellipsometric Fourier scatterometry, the amplitude and phase of the input field does not have to be measured. A sensitivity increase can be achieved also for gratings without overlapping orders. The hardware is the same as for a basic scanning spot configuration, but no scanning is required. However, the polarizer at the input or output side has to be rotated and the intensity modulation at each pixel of the CCD has to be measured, which makes the data acquisition slower, and requires additional calculation to determine the complex reflectance ratio. Since the polarizer of most modern ellipsometers rotates at a speed of up to 20 Hz, data acquisition is not a considerable limitation, especially compared with the computation need for solving the inverse problem of periodic structures. In order to achieve the usual accuracy of 0.05° for the phase (Δ of Eq. 1) measurement in ellipsometry, the polarizer offset has to be calibrated using measurements on reference samples. A further significant advantage of the ellipsometric method is that no coherent light source is needed, and therefore the method can relatively easily be upgraded to a spectroscopic version.

Table 1: Advantages and disadvantages of different Fourier scatterometry approaches compared to incoherent Fourier scatterometry.

Method	Advantages	Disadvantages
Scanning spot	Nanopositioning Phase between orders	Input intensity measurement needed
Interferometry	Nanopositioning No overlapping orders needed	Input intensity measurement needed Additional hardware elements
Ellipsometry	No input wavefront measurement needed No overlapping orders needed Simple hardware No coherent source needed Spectroscopy can be realized Nanopositioning also possible if coherent source is used	More computation Offset calibration

Conclusions

It was shown that similar to the scanning focused spot and interferometric methods, the phase information determined using ellipsometry in Fourier scatterometry increases the sensitivity significantly. The advantages of ellipsometry over other approaches are that a simple hardware can be used, there is no need to measure the input wavefront parameters, incoherent illumination is sufficient, enabling the use of spectroscopy with conventional light sources.

Acknowledgments

Support from EMRP IND17 joint research project on scatterometry and ENIAC E450EDL are greatly acknowledged for financial support. The EMRP is jointly funded by the EMRP participating countries within EURAMET and the European Union.

REFERENCES

[1] B. Bodermann, E. Buhr, H.-U. Danzebrink, M. Bär, F. Scholze, M. Krumrey, M. Wurm, P. Klapetek, P.-E. Hansen, V. Korpelainen, M. van Veghel, A. Yacoot, S. Siitonen, O. El Gawhary, S. Burger, and T. Saastamoinen, "Joint Research on

Scatterometry and AFM Wafer Metrology", AIP Conference Proceedings **1395** 319 (2011).

[2] B. Bodermann, P.-E. Hansen, S. Burger, M.-A. Henn, H. Gross, M. Bär, F. Scholze, J. Endres, and M. Wurm, "First steps towards a scatterometry reference standard", SPIE Proceedings **8466** 84660E–1 (2012).

[3] V. F. Paz, S. Peterhänsel, K. Frenner, and W. Osten, "Solving the inverse grating problem by white light interference Fourier scatterometry", Nature Light: Science and Applications **1** e36 (2012).

[4] N. Kumar, P. Petrik, G. K. P. Ramanandan, O. El Gawhary, S. Roy, S. F. Pereira, W. M. J. Coene, and H. P. Urbach, "Reconstruction of sub-wavelength features and nano-positioning of gratings using coherent Fourier scatterometry", Optics Express **22** 24678 (2014).

[5] P. Boher, J. Petit, T. Leroux, J. Foucher, Y. Desières, J. Hazart, and P. Chaton, "Optical Fourier Transform Scatterometry for LER and LWR metrology", SPIE Proceedings **5752** 192 (2005).

[6] N. Kumar, O. El Gawhary, S. Roy, S. F. Pereira, and H. P. Urbach, "Phase retrieval between overlapping orders in coherent Fourier scatterometry using scanning", J. Europ. Opt. Soc. Rap. Public. **8** 13048 (2013).

[7] O. El Gawhary, N. Kumar, S. F. Pereira, W. M. J. Coene, and H. P. Urbach, "Performance analysis of coherent optical scatterometry", Applied Physics B **105** 775–781 (2011).

[8] S. Roy, N. Kumar, S. F. Pereira, and H. P. Urbach, "Interferometric coherent Fourier scatterometry: a method for obtaining high sensitivity in the optical inverse-grating problem", Journal of Optics **15** 075707 (2013).

[9] H. Fujiwara, *Spectroscopic Ellipsometry: Principles and Applications* (Wiley, New York, 2007).

[10] M. Losurdo and K. Hingerl, *Ellipsometry at the Nanoscale* (Springer-Verlag, Heidelberg, 2012).

[11] H. G. Tompkins and E. A. Irene, *Handbook of Ellipsometry* (William Andrew Publishing, 2005).

[12] N. Kumar, *Coherent Fourier Scatterometry*, Ph.D. thesis, Technical University Delft (2014).

[13] N. Kumar, O. El Gawhary, S. Roy, V. G. Kutchoukov, S. F. Pereira, W. Coene, and H. P. Urbach, "Coherent Fourier scatterometry: tool for improved sensitivity in semiconductor metrology", Control **8324** 83240Q–83240Q–8 (2012).

[14] S. Roy, O. El Gawhary, N. Kumar, S. F. Pereira, and H. Urbach, "Scanning effects in coherent fourier scatterometry", J. Europ. Opt. Soc. Rap. Public. **7** (2012).

[15] M. G. M. M. van Kraaij, *Forward Diffraction Modelling: Analysis and Application to Grating Reconstruction*, Ph.D. thesis, Technische Universiteit Eindhoven (2011).

[16] W. H. Press, S. A. Teukolsky, W. Vetterling, and B. P. Flannery, *Numerical recipes in C, The art of scientific computing* (Cambridge University Press, 1995).

[17] C. M. Herzinger, P. G. Snyder, B. Johs, and J. A. Woollam, "InP optical constants between 0.75 and 5.0 eV determined by variable-angle spectroscopic ellipsometry", J. Appl. Phys. **77** 1715 (1995).

[18] J. Pomplun, S. Burger, L. Zschiedrich, and F. Schmidt, "Adaptive finite element method for simulation of optical nano structures", phys. stat. sol. b **244** 3419 (2007).

[19] S. Burger, L. Zschiedrich, J. Pomplun, F. Schmidt, and B. Bodermann, "Fast simulation method for parameter reconstruction in optical metrology", SPIE Proceedings **8681** 868119 (2013).

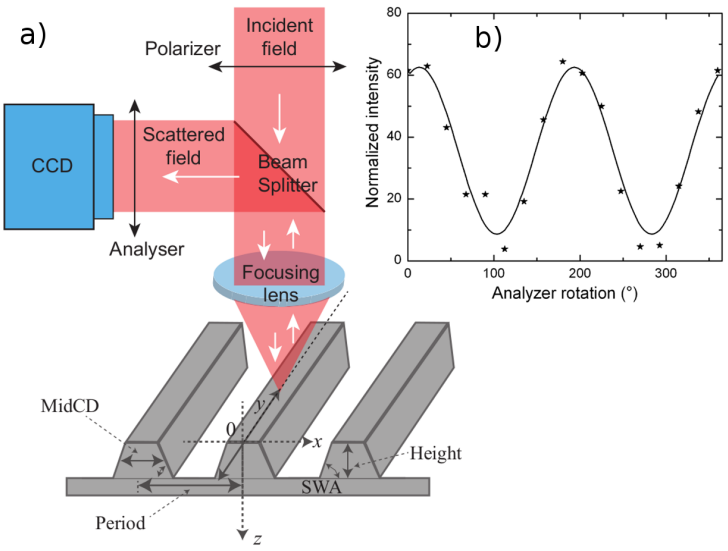

Figure 1: (a) Setup of ellipsometric Fourier scatterometry. (b) Intensity signal at an arbitrary pixel of the CCD as a function of polarizer rotation at the output side.

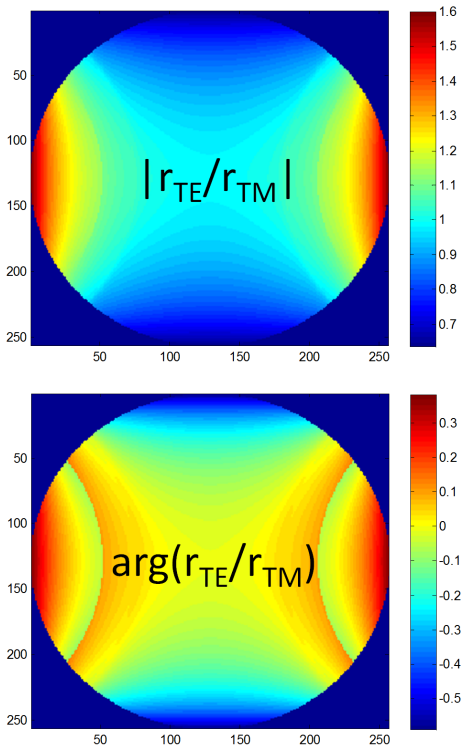

Figure 2: Absolute values ($|r_{TE}/r_{TM}|$) and phases ($arg(r_{TE}/r_{TM})$ in radian) of the ratio of complex reflection coefficients (r) of light polarized parallel (TE) and perpendicular (TM) to the grating lines for x and y coordinates spanning the whole NA=0.9 pupil area. The parameters of the grating used for the calculation are: height = 40 nm, pitch = 300 nm, critical dimension = pitch/2, wavelength = 405 nm, and NA = 0.9. The material of the grating lines and the substrate are resist ($n = 1.45$ at the wavelength of $\lambda = 405$ nm) and silicon ($n = 5.42 + 0.329i$ at $\lambda = 405$ nm), respectively, where n and λ denote complex refractive index and the wavelength of illumination.

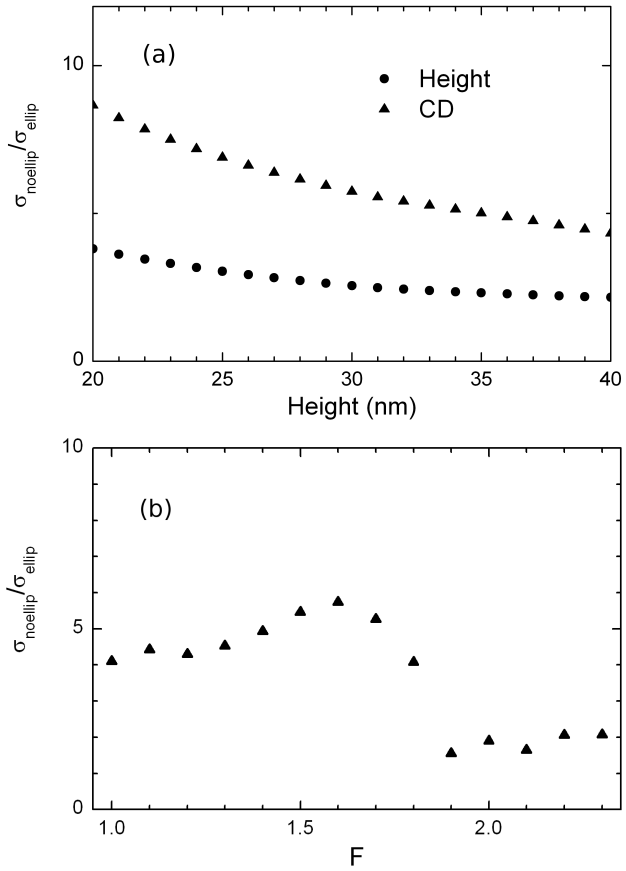

Figure 3: Ratios of parameter uncertainties calculated from the derivatives of the merit function (sum of squared differences of far field pupil values for each pixel of Fig. 2 for varied parameters) with (σ_{ellip}) and without ($\sigma_{noellip}$) the ellipsometric approach as a function of grating parameters of height and critical dimension (CD - graph (a)) as well as a function of the overlap parameter ($F = \lambda/(NA \times \Lambda)$, where λ and Λ denote the wavelength of illumination and the pitch, respectively, see graph (b)). The parameters of the grating used for the calculation are: height = 40 nm, pitch = 300 nm, critical dimension = pitch/2, wavelength = 405 nm, and NA = 0.9. The material of the grating lines and the substrate are resist ($n = 1.45$ at $\lambda = 405$ nm) and silicon ($n = 5.42 + 0.329i$ at $\lambda = 405$ nm), respectively, where n and λ denote complex refractive index and the wavelength of illumination.

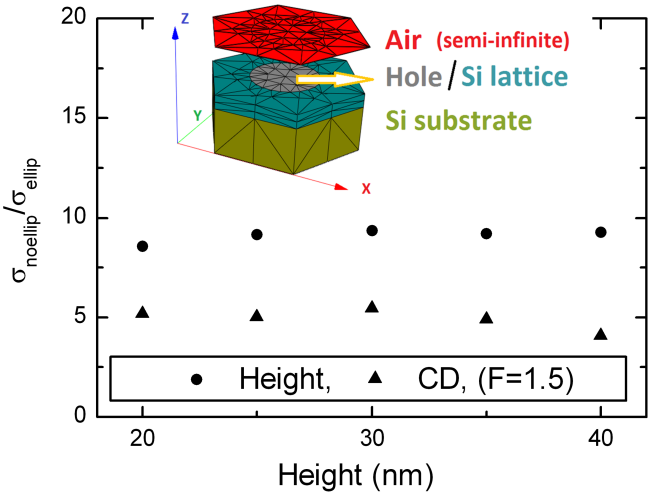

Figure 4: Ratios of parameter uncertainties calculated from the derivatives of the merit function (sum of squared differences of far field Ψ and Δ values along the x-z plane shown in the inset, for illumination and reflection angles steped by 3° in the range of 0-63°, corresponding to a numerical aperture of 0.9, calculated for varied model parameters) with (σ_{ellip}) and without ($\sigma_{noellip}$) the ellipsometric approach. The inset shows the computational domain. The sample consists of these domains as unit cells attached in a hexagonal order with a pitch (Λ) of 300 nm, critical dimension of $\Lambda/2$, wavelength of 405 nm, and numerical aperture of 0.9.